ADVANCED MATERIALS
www.advmat.de

Supramolecular Architectures of Dendritic Polymers Provide Irreversible Inhibitor to Block Viral Infection

Ehsan Mohammadifar, Matteo Gasbarri, Mathias Dimde, Chuanxiong Nie, Heyun Wang, Tatyana L. Povolotsky, Yannic Kerkhoff, Daniel Desmecht, Sylvain Prevost, Thomas Zemb, Kai Ludwig, Francesco Stellacci,* and Rainer Haag**

In Nature, most known objects can perform their functions only when in supramolecular self-assembled from, e.g. protein complexes and cell membranes. Here, a dendritic polymer is presented that inhibits severe acute respiratory syndrome coronavirus 2 (SARS-CoV-2) with an irreversible (virucidal) mechanism only when self-assembled into a Two-dimmensional supramolecular polymer (2D-SupraPol). Monomeric analogs of the dendritic polymer can only inhibit SARS-CoV-2 reversibly, thus allowing for the virus to regain infectivity after dilution. Upon assembly, 2D-SupraPol shows a remarkable half-inhibitory concentration (IC_{50} 30 nM) in vitro and in vivo in a Syrian Hamster model has a good efficacy. Using cryo-TEM, it is shown that the 2D-SupraPol has a controllable lateral size that can be tuned by adjusting the pH and use small angle X-ray and neutron scattering to unveil the architecture of the supramolecular assembly. This functional 2D-SupraPol, and its supramolecular architecture are proposed, as a prophylaxis nasal spray to inhibit the virus interaction with the respiratory tract.

1. Introduction

Developing new methods for the preparation of Two-dimmensional supramolecular polymers with controlled and uniform dimensions has been of great interest in biomedical applications, but still remains challenging.[1] This research avenue is compelling because biological properties of nanomaterials are influenced by their spatial features.[2] Supramolecular structures are particularly intriguing as they are inspired by nature. Cell membranes, self-assembled from amphiphilic phospholipids, are a good example of the advantages of dynamic 2D supramolecular structures in biological systems, enabling cells to sense micro-environments and change morphology adaptively. Since supramolecular assemblies rely primarily on non-covalent interactions like hydrogen bonding, electrostatic interactions, and hydrophobic interactions, they can contribute multivalently at bio-interfaces that offer sites for such interactions.[3] Additionally, they can engage in numerous weak non-covalent bindings, resulting in strong yet dynamic multivalent interactions.

Multivalency has already shown its potential in biomedical applications, leading in the 1960s to the development of a new class

E. Mohammadifar, C. Nie, T. L. Povolotsky, R. Haag
Institut für Chemie und Biochemie Freie Universität Berlin
Takustr 3, 14195 Berlin, Germany
E-mail: haag@zedat.fu-berlin.de

M. Gasbarri, H. Wang, F. Stellacci
Institute of Materials
École Polytechnique Fédérale de Lausanne (EPFL)
Lausanne 1015, Switzerland
E-mail: francesco.stellacci@epfl.ch

M. Dimde, Y. Kerkhoff, K. Ludwig
Forschungszentrum für Elektronenmikroskopie und Gerätezentrum BioSupraMol
Institut für Chemie und Biochemie
Freie Universität Berlin
Berlin, Germany
E-mail: kai.ludwig@fzem.fu-berlin.de

The ORCID identification number(s) for the author(s) of this article can be found under https://doi.org/10.1002/adma.202408294

D. Desmecht
Animal Pathology
FARAH Research Center
Faculty of Veterinary Medicine
University of Liège
Sart-Tilman B43, Liège 4000, Belgium

S. Prevost
Institut Laue-Langevin – The European Neutron Source
71 avenue des Martyrs – CS 20156 38042, Grenoble cedex 9, France

T. Zemb
ICSM
CEA
CNRS
ENSCM
Univ Montpellier
Bagnols-sur-Ceze 30207, France

DOI: 10.1002/adma.202408294

of antiviral materials known as broad-spectrum viral inhibitors.[4] Unlike traditional medicinal drugs that act specifically against certain viruses, broad-spectrum antivirals can target a range of viruses from different subclasses that utilize the same receptor for host cell entrance.[5] In principle, these antivirals interact with viruses in a non-specific and multivalent manner, blocking the early stage of virus-host interaction regardless of antigenic evolution.[6] Unfortunately, the translation into the clinic of these antiviral molecules has been hindered by their mechanism that, being based of (multivalent) binding, is intrinsically reversible (virustatic); thus, upon dilution of the molecules, the non-infective virus-molecules complex dissociates leaving a infective virus to restart its infection cycles. There are many known broad-spectrum molecules that can irreversibly inhibit viral infection (virucidal mechanism), for example alcohols, surfactants, and acids. Unfortunately, most known virucidal molecules are toxic to host cells almost as much as they are to viruses.[7] Recently, we have shown that it is possible through careful molecular design to synthesize virucidal antivirals that are non-toxic to the host. This can be achieved by modifying the design of multivalent virustatic drugs with the addition of relatively long hydrophobic moieties.[8]

During COVID-19, numerous multivalent inhibitors have been developed, with a particular focus on biomaterials such as multivalent nanobodies,[9] proteins,[10] peptides,[11] cellular nanosponges,[12] oligonucleotides,[13] antibodies,[14] and various types of inorganic and polymeric nanostructures.[15] However, these inhibitors are constrained by a virustatic inhibition mechanism. We have shown that including a combination of sulfate/sulfonate groups and long hydrophobic alkyl chain in the inhibitors' structures endows them with a virucidal mechanism against several virus types.[8] However, against SARS-CoV-2 these materials showed only virustatic (reversible) and not virucidal (irreversible) inhibition.[16] In this work, we design a virus inhibitor based on isolated dendritic polymer functionalized with long hydrophobic chains that self-assemble in 2D supramolecular polymers in physiological solutions. Unlike its isolated analogs, 2D-SupraPol with similar hydrophobic content, as the isolated monomers, binds to SARS-CoV-2 in a virucidal (irreversible) mechanism, highlighting the functional advantage of supramolecular polymers.

2. Results and Discussion

2.1. Polymer Synthesis and Characterization

In this study, we synthesized an amphiphilic dendritic polymer that can self-assemble in solution into well-defined and monodisperse nanosheets with controllable lateral size. Dendritic polymers have shown promising potential in nanomedicine.[17] We used dendritic polyglycerol (dPG) as a nanoscale multivalent platform due to its flexible and globular structure, with abundant terminal hydroxyl groups enabling further functionalization with ligands of interest (Figure S1, Supporting Information). Knowing that dPG-based macromolecules with different functionalities can adhere multivalently to pathogens,[18] we hypothesized that combining long aliphatic chain with terminal carboxylic acid groups would boost the multivalent interaction of dPG and SARS-CoV-2. (This interaction is mostly triggered by H-bonding, electrostatic, and hydrophobic interaction, as they are the most important molecular interactions between the viral receptor-binding domain (RBD) and the host-cell ACE2.[19]) Toward this goal, highly branched dPG with a molecular weight of 10 kDa was fully functionalized with a high density of 11-mercaptoundecanoic acid (MUA) as peripheral ligands. The reaction was performed in a gram-scale synthesis, consisting of two steps of reaction of dPG with allyl bromide, followed by thiol-ene click chemistry of MUA resulting in dPG-MUA (Figure S2, Supporting Information; Figure S3). ^{1}HNMR data showed that the dPG-MUA macromolecule is functionalized and has ≈135 undecanoic acid groups. The undecanoic ligands are randomly distributed inside the core backbone and exposed on the surface of the polymer. Treating the dPG as a sphere with hydrodynamic size of 4 nm, the average ligand density is calculated at 1.6 ligands per nm^2 by dividing the number of undecanoic acid groups by the surface area. The full characterization of dPG-MUA, and the and reaction steps to create it, are presented in Figure S3, supporting information and **Figure 1**.

2.2. 2D Supramolecular Polymer (2D-SupraPol) Formation

Generally, the formation of supramolecular structures, and therefore their size and morphology, are highly dependent on the pH and ionic strength of the solution. This dependency makes the development of supramolecular structures for biological applications extremely challenging, given the specificity of the biological milieu.[20] Therefore, the development of macromonomers that can form 2D self-assemblies in physiological pH and ionic strength is a highly sought-after goal in biological applications.[21] Crucially, dPG-MUA self-assembles in a well-defined 2D supramolecular nanostructure in phosphate buffered saline (PBS) having pH 7.4 and ionic strength of 152.7 mM in a time-dependent manner. 2D-SupraPol is, like other supramolecular systems, sensitive to pH and ionic strength, as well as polymer concentration. Therefore, the lateral size and morphology of 2D-SupraPol can be tuned by changing the pH of solution. The balance between attractive and repulsive forces is the mechanism of 2D-SupraPol's tunable size and morphology. The hydrogen bonds of carboxylic acid groups and hydrophobic interaction between aliphatic chains are the attractive forces, while the electrostatic repulsion of negatively charged surfaces, originating with the carboxylate groups, works to prevent aggregation. The balance between attractive and repulsive forces can be disturbed, and can therefore be controlled, by small changes in pH and ionic strength. These changes can alter the size and morphology of 2D-SupraPol, or even lead to its complete disassembly. Moreover, long aliphatic chains cannot protrude in water, and they therefore, form a dense layer of fluid analogue in the center of 2D-SupraPol bilayers via the hydrophobic effect. After replacement of undecanoic acid (C_{10}-COOH) by less hydrophobic octanoic acid (C_7-COOH) (Figure S4, Supporting Information) no aggregation was observed at similar pH and ionic strength. The formation of 2D-SupraPol also depends on polymer concentration, as we observed no self-assembly at 5 mg mL^{-1} of dPG-MUA 24 h after solution preparation while keeping the pH and ionic strength constant. (Figure S7, Supporting Information).

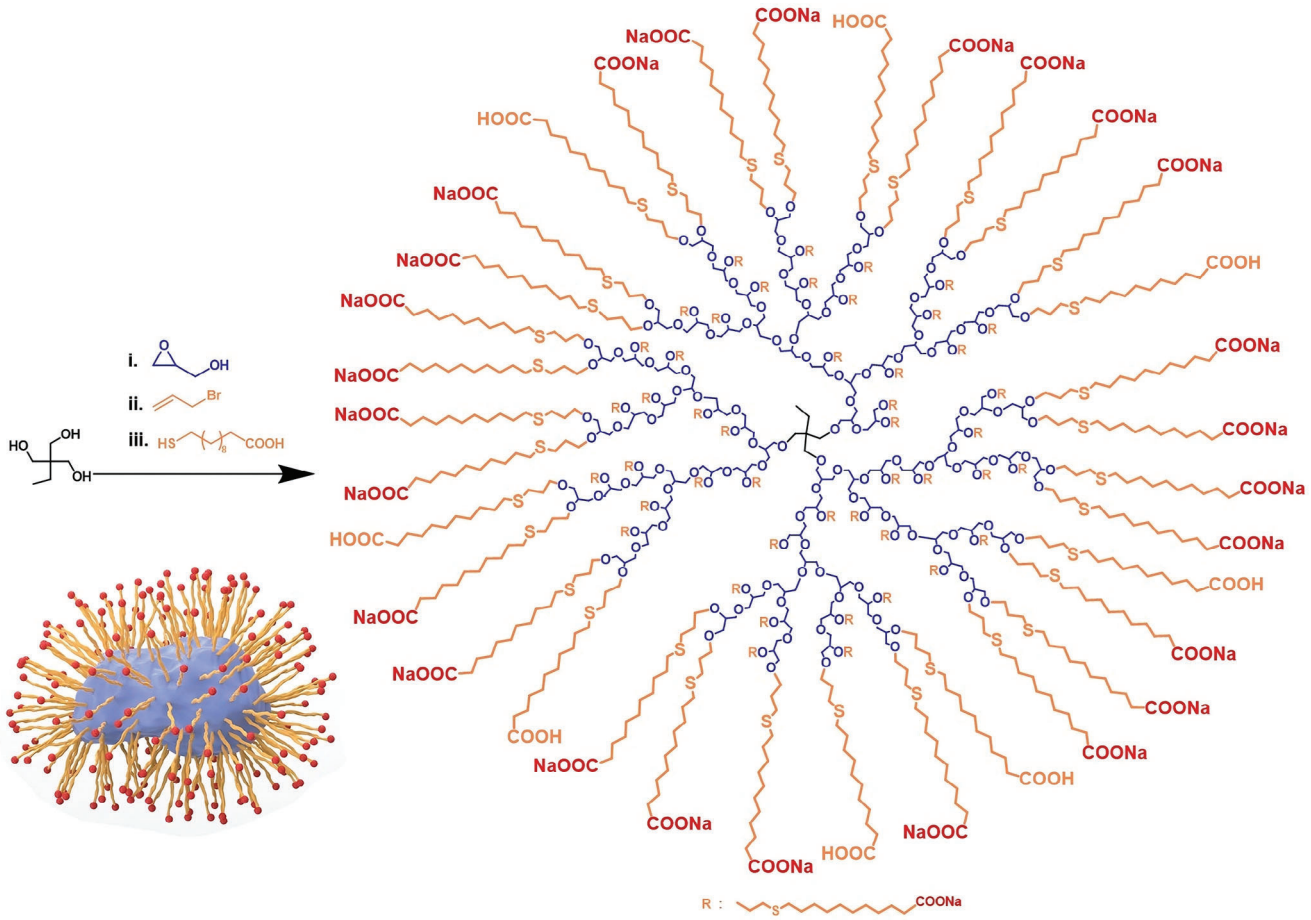

Figure 1. Synthetic route and structure of dPG-MUA. The dPG-MUA is synthesized through three sequential reactions. i) Synthesis of dendritic polyglycerol through ring opening polymerization of glycidol ii) Functionalization of hydroxyl groups via nucleophilic substitution of allyl bromide to have allyl groups which will be used for iii) Conjugation of 11-mercaptoundecanoic acid via UV-initiated thiol-ene click chemistry. The inset shows the schematic 3D representation of dPG-MUA. The ^{1}HNMR characterization of the product in each step and signal assignment is shown in Figure S3, (Supporting Information).

The lateral size growth of nanosheets was observed by cryo-TEM imaging at different time intervals. As seen in **Figure 2**, after dissolving the polymer in PBS, 2D supramolecular structures began to form and grow in a time-dependent manner. In the first two hours, the nanosheets were flat and showed broad size dispersity, but after four hours, imaging showed objects of larger lateral size, containing wrinkles and folded areas due to their high flexibility. After 24 h, the 2D-SupraPol assemblies with narrow size dispersity as well as more wrinkles and folded edges have been observed. The 3D morphology of the folded and intertwined nanosheets in solution was visible by cryo-electron tomography (cryo-ET) analysis, and their lateral size 1, 2, 4, and 24 h after solution preparation was approximately estimated to be 65, 80, 140, and 250 nm respectively. The zeta-potential measurement of 2D-SupraPol revealed the negative surface charge of −35 mV. The size and structural scaffold of 2D-SupraPol are strongly dependent on pH, so that a pH increase of 0.1 leads to the formation of smaller structures in the form of nanodiscs (**Figure** 3a–c). This is due to the deprotonation of carboxylic acid and the formation of negatively charged carboxylate groups. The electrostatic repulsion forces between carboxylate groups disrupts the balance between attractive and repulsive forces, resulting in smaller structures. Deprotonation of carboxylic acid also decreases the possibility of H-bond formation.[22] The hydrophobic C10-carboxylic acid groups tend to form in-plane hydrogen bonds, resulting in lower exposure to water, while the hydrophilic carboxylate groups present on the surface.[23] The negative surface charge originating from the carboxylate groups serves as the repulsive force between 2D-SupraPol assemblies, preventing aggregation in a stable colloidal solution.

Further investigations and electron micrographs taken close to the focus show that 2D-SupraPol has a membrane-like bilayer structure (Figure 3; Figure S8, Supporting Information). We assume that the hydrophobic chains are imbedded in the middle of layers due to repulsion by water. The strong hydrophobic effect between the aliphatic chains in the mid-layer area of the assembly, in combination with the properties of the surface layer in contact with water, forms the basis of 2D-SupraPol's stability after reaching equilibrium size.

To further investigate the detailed molecular architecture of 2D-SupraPol, we studied it in stable colloidal suspension by conjunction of ultra-small angle X-ray scattering (USAXS) and small

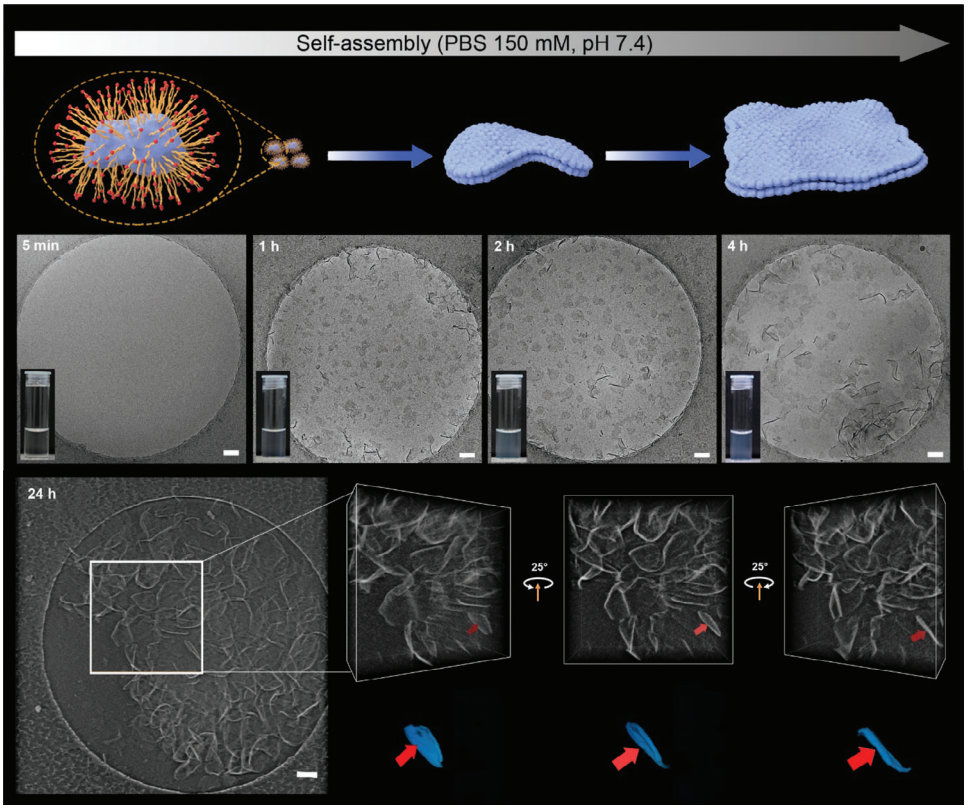

Figure 2. dPG-MUA macromonomers self-assemble in ultra-thin nanosheets in PBS solution in a time-dependent manner. The samples for cryo-TEM measurement have been plunge-frozen at different time intervals after dissolving the dPG-MUA in PBS. The insets show the solutions after the same time intervals corresponding to the respective micrograph. The lateral size of 2D-SupraPol is increasing over time. A cryo-electron tomogram was taken after 24 h (bottom left). The three figures at bottom-right show an enlarged view of the reconstructed 3D volume, rotated by 25°, 0°, and −25° around the y-axis, respectively. The scale bars in all images are 100 nm.

angle neutron scattering (SANS), with a dynamic range in scattering cross-section over four decades in intensity. The scattered intensities measured for a sample at 1 mg mL^{-1} in H_2O for SAXS and D_2O for SANS, both in phosphate-based buffer and at pH = 7.5 (Figure S9, Supporting Information). In the intermediate q-range, the slope is q^{-2}, indicating 2D objects in the absence of repulsive interaction of steric or electrostatic origin.[24] This general trend in SANS and SANS decays, with scattering vector q^{-2} over two decades, demonstrates the existence of flat sheets.[25]

Applying a Guinier fit to the Kratky representation of data (Iq^2 versus q) leads to disk thicknesses of 7.5 nm for SAXS and 4 nm for SANS. SAXS is sensitive to electron density, i.e., also counter-ions, and the SAXS thickness therefore includes the hydrated layer.[26] The effective thickness is larger because the bilayer is heterogenous: some parts have lower electron density than the buffer due to the hydrocarbon chains, and some layers have a higher electronic density. The form-factor oscillations seen in SAXS (Figure S9a, Supporting Information) need to be modeled with a heterogeneous structure, considering the known molecular polymer volume (71.5 nm^3) and number of electrons per polymer (23 000). In the high-resolution q-range between 2 and 5 nm^{-1}, the signal shows complex oscillations. Several sub-layers present in 2D-SupraPol need to be considered in order to determine the distribution of electron densities responsible for these oscillations. A symmetric step profile with 7 sub-layers reproduces the complex pattern observed and is consistent with the illustrated model proposed for the self-assembly, as well as with the EM data; the resulting scattering length density profile is presented in Figure 3g. The artistic view of the self-assembly superimposed on the EM image shows the agreement between the double-layer model and the image obtained; this is confirmed with the comparison between the cross-section electron density as derived from EM and the cross-section density as obtained by the best fit of SAXS data. This best fit is presented with experimental curve in a Kratky plot designed to focus on the high-q oscillations (Figure S9b, Supporting Information). Two outer diffuse layers rich with sodium as a counter-ion cloud (0.5 nm) are seen in SAXS but not in SANS. The net negative structural charge, only partially compensated for sodium cations, electrostatically stabilizes two stretched monolayers of MUA of thickness 0.8 ± 0.1 nm of lower electronic density than the buffer with added salt; two dPG cores, of thickness 2 ± 0.2 nm, have higher electronic density than water. The volume of the non-functionalized dPG core is known to be the same as a sphere of 4 nm diameter when no stress deforms those spheres. Under stress and in self-assembled double-layers, they are probably deformed as oblate ellipsoids of thickness of 2 nm when observed from the side: these layers (DC) are a hybrid material made principally from dPG (25%) and grafted MUA (75%) of 2 nm and the central layer made from hydrophobic phase with carboxylic

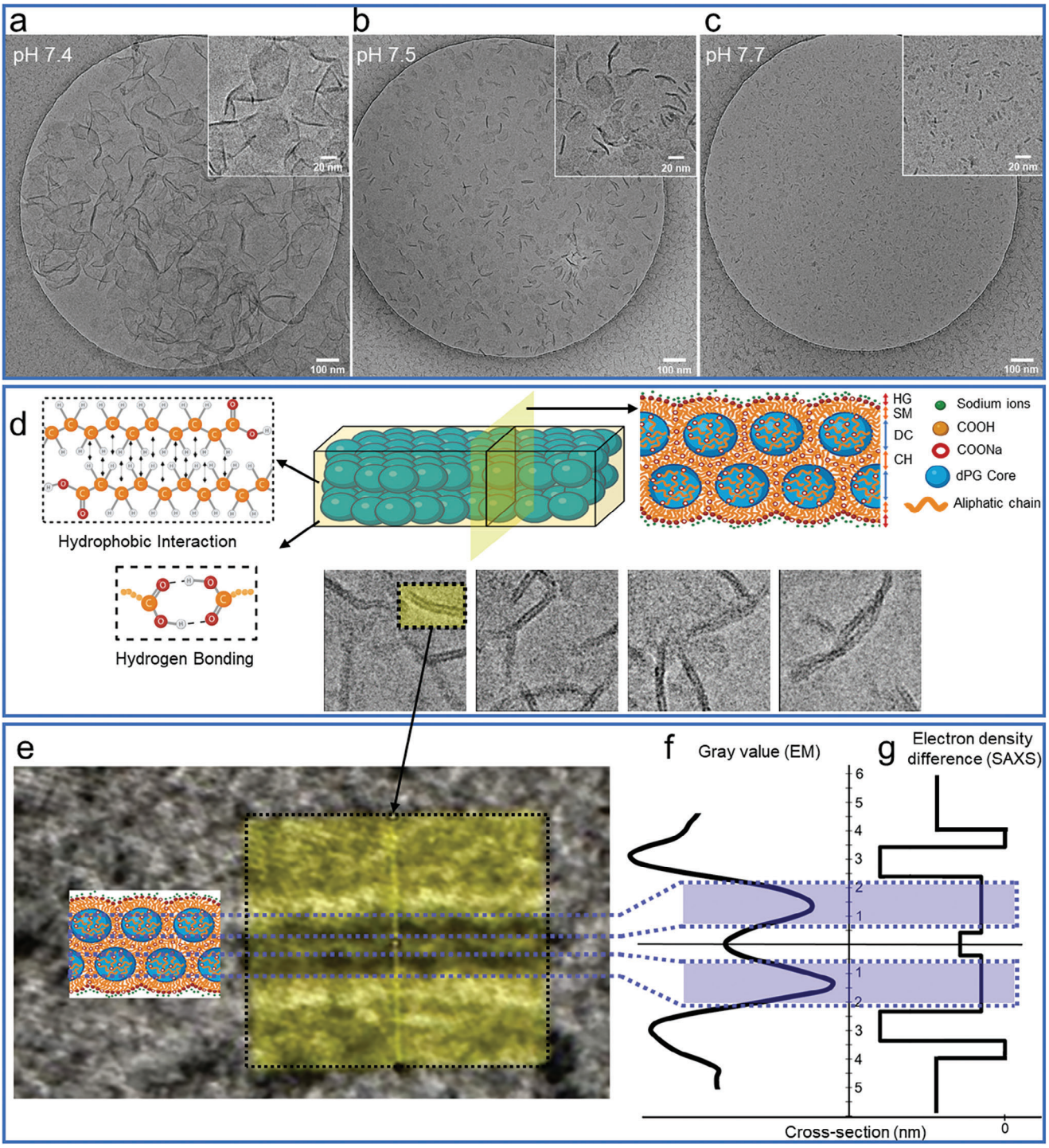

Figure 3. The effect of medium pH on the size and structure and the proposed model for 2D-SupraPol. Cryo-TEM images of 2D-SupraPol prepared at different pH values. The solutions were prepared in PBS at a concentration of 1 mg mL^{-1}, and the images were recorded 24 h after solution preparation. pH of solutions is adjusted to a) 7.4, b) 7.5, and c) 7.7. The inset shows the zoomed-in view of images. D) Schematic representation and cryo-TEM of the proposed model of 2D-SupraPol and its cross-section view. Cryo-TEM images of 2D-SupraPol embedded vertically in amorphous ice and acquired close to the focus to illustrate the double-layer morphology (The size of cryo-TEM images is 100×100 nm). The driving force of self-assembly is mostly based on the hydrogen bonding and hydrophobic interaction. The sublayers shown in the model are described as; T_{HG} for thickness of hydrated charged head groups and counter-ion, T_{SM} for the thickness of the surface stretched MUA layer, T_{DC} for the thickness of dendritic core layer, T_{CH} for the central cross-linked hydrocarbon layer. E) cryo-TEM image of the cross-section of 2D-SupraPol f) the gray value plotted from the cross-section cryo-TEM g) the difference in scattering length density with the solvent (ΔSLD) as accessible by high-res SAXS.

acid groups (CH) acting as linkers of two layers.[27] This layer has a thickness of 1.1 nm ± 0.2 nm with less electron density than the buffer. The finite total thickness of 2D-SupraPol bilayers is 7 ± 0.3 nm. The low total thickness comes from a mismatch between excess carboxylate area (60 nm^2 per polymer for 135 carboxylate groups per dPG) and the effective area of contact with water (20 nm^2 per polymer).

In order to assess its stability, 2D-SupraPol was prepared in PBS solution at concentration of 1 mg mL^{-1} and the solution was diluted to 1 µg mL^{-1} with either PBS or distilled water. The size distribution and concentration (particles mL^{-1}) of diluted samples were measured by nanotracking analysis (NTA). As the NTA data shows (Figure S10, Supporting Information) the particle size of the 2D-SupraPol diluted in distilled water is smaller than those of diluted in PBS. The Brownian motion of the individual 2D-SupraPol in solution, as measured by NTA, is shown in the Video S2 (Supporting Information).

2.3. 2D-SupraPol Inhibits SARS-CoV-2 In Vitro and In Vivo

So far, several polymer-based materials functionalized with sulfate and sulfonate groups have shown infection inhibition against SARS-CoV-2, probably due to their ability to mimic heparan sulfates, which are a key moiety of the cell-membrane glycans that interact with many viruses.[28] We functionalized the multivalent dPG with carboxylate groups to mimic the electrostatic interaction between negatively charged nanomaterials and positively charged residues on S-protein of SARS-CoV-2 that facilitates virus binding.[19,29] We also included long hydrophobic chains in the structure to equip the compound for irreversible virus inhibition via stronger interaction with the virus envelope.[30] Considering the ability of dPG–MUA in forming supramolecular interactions, and being aware of hydrophobic, polar, and positively charged residues on the RBD of S-protein of SARS-CoV-2, we hypothesized that the functional groups of RBD ($-NH_3^+$, –OH, $-CONH_2$, $-C_6H_5$, $-CH_3$, and –SH) can potentially interact with the supramolecular structures. The inhibitory effect of 2D-SupraPol against SARS-CoV-2 showed a dose-dependent manner with IC_{50} = 30 nM (1 µg mL^{-1}), and virucidal activity (≈two order of magnitude decrease of viral titer) was observed (Figure 5). The cell viability assay showed that the polymer has low cytotoxicity with the CC_{50} higher than 1 mg mL^{-1} on three different cell lines (A549, HBE, and Vero E6) referring to a selectivity index (SI) of higher than 1000 (SI, the ratio between cytotoxic, CC_{50} and antiviral concentrations, IC_{50}). In order to investigate the effect of supramolecular assembly in virus inhibition, we produced many similar compounds that lacked the ability to self-assemble. First, dPG was functionalized with carboxylic acid groups having shorter chains (7 and 2 carbons) since they stay as isolated monomers in solution and do not form assemblies (Figures S4 and S5, Supporting Information, respectively), this compound did not show any detectable viral inhibition. Then we synthesized a dendritic polymer in which the entire structure of dPG-MUA was kept the same, but carboxylates were replaced by sulfonate groups (dPG-MUS) (Figure S6, Supporting Information). It should be noted that dPG-MUS showed no supramolecular self-assembly. Although the dPG-MUS showed an activity in virus inhibition (EC_{50} of 6.8 µg mL^{-1}) that was comparable to dPG-MUA, it was not virucidal and only showed a reversible mechanism (Figures S13–S15, Supporting Information). To further elucidate the role of supramolecular self-assembly in the virucidal behavior, we tested MUA functionalized cyclodextrins, they showed a comparable EC_{50} of 4 µg mL^{-1} but only a reversible mechanism.[31] Thus, we postulate that the virucidal mechanism of dPG-MUA is an effect of the supramolecular structures. Indeed, the supramolecular assemblies are also virucidal against other types of virus such as HSV-2 even though they show lower interaction affinity.[31] These findings prove that a supramolecular architecture does not need to bind to a virus very strong (low EC50) to be irreversible since numerous weak multivalent interactions facilitate the irreversible binding.

In the presence of virus, the self–assemblies assemble on the virus envelope or spike protein. The RBD of the spike protein of SARS-CoV-2 has an abundance of amino acid residues with the potential for H-bonding, hydrophobic, and electrostatic interactions[19,32] and therefore can initiate the supramolecular interaction with dPG-MUA. The planar β-sheet structure together with the positively charged patch of RBD, strengthens the hypothesis of high binding affinity of 2D-SupraPol to the RBD.[32–33] The binding affinity of 2D-SupraPol with the ectodomain (S1 + S2) of S-protein of SARS-CoV-2 was measured by microscale thermophoresis (MST) to be 2.2 µM (Figure S11, Supporting Information). The detailed interaction of 2D-SupraPol and SARS-CoV-2 was further investigated and visualized by cryo-TEM and cryo-ET after incubation of dPG-MUA and virus solution for 1 and 24 h (**Figure 4**; Figure S12 and Video S3, Supporting Information).

Given the results obtained in vitro, we designed an in-vivo study to confirm the efficacy of 2D-SupraPol as an effective antiviral against SARS-CoV-2, using hamsters as an animal model via intranasal administration. The efficacy of antivirals was assessed in two different doses (1.5 mg kg^{-1} day^{-1} and 4.5 mg kg^{-1} day^{-1}). The polymer solution was administered through nostrils under brief but deep gas anesthesia to avoid sneezing and coughing. As seen in **Figure 5**e, the weight of the control group increased during the 15 days, showing no effect due to either the anesthesia or the intranasal administration of PBS. The placebo group, which was infected but received only PBS for 5 days, showed high loss of body weight up to day 6, after which it recovered, regaining its original weight at day 12. The body weight loss averaged ≈20% at day 6. For the two groups that received 2D-SupraPol, we detected dose-responsive behavior. In fact, the lower dose showed no antiviral effect, with the body weight curve basically overlapping with the placebo group. The higher-dose (4.5 mg kg^{-1} day^{-1}) group, which received 3 times the dose of the lower-dose group, showed a clear difference compared to placebo. In fact, while this group's weight loss up to day 6 was comparable to the placebo group, the recovery seemed to accelerate after the administration of 2D-SupraPol. In fact, between day 6 and day 10, the higher-dose group's body weight loss was lower than the placebo group, indicating a possible positive effect due to the compound. Additionally, histopathology studies were performed on the animals at the end of the study. These studies detected no detrimental effects from possible toxicity, supporting the non-toxicity of the compound.

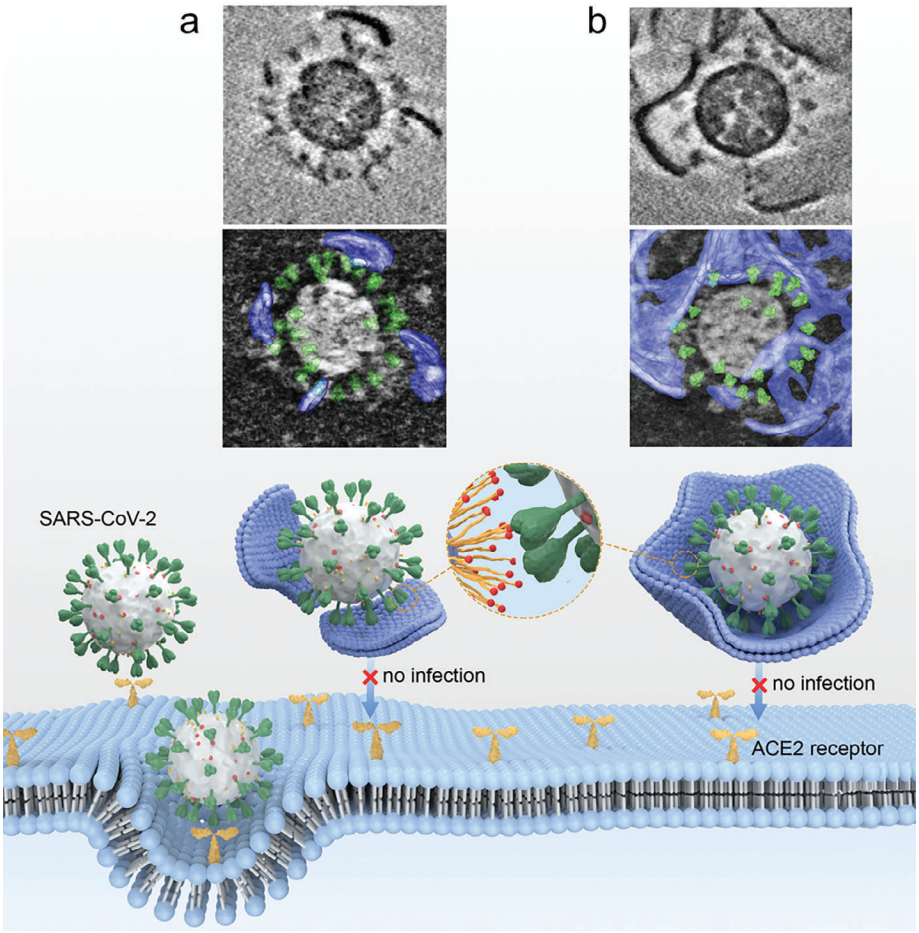

Figure 4. Representation of the interaction of 2D-SupraPol with virus particles of SARS-COV-2. Cryo-electron tomogram taken after a) 1 h and b) 24 h after incubation of dPG-MUA with SARS-COV-2. On top, a single orthoslice of the 3D calculated from the tilt angle series is shown, below the voltex presentation of the volume with the 3D model obtained as a result of the tomogram segmentation (transparent overlay, spike proteins shown in green and 2D-SupraPol in blue). Schematic of the interaction of 2D-SupraPol with virus which results in inhibition of cell entry is shown at the bottom part of figure.

3. Conclusion

We developed a biocompatible antiviral polymer of tunable size and morphology. This polymer, 2D-SupraPol, is based on an amphiphilic dendritic polyglycerol that self-assembles into uniform and narrowly size-dispersed 2D supramolecular polymers in aqueous media at physiological conditions (pH 7.4 & salt concentration 152.7 mM). The size and morphology of 2D-SupraPol can be tuned via the pH of the solution: we controlled the supramolecular polymers' lateral size from 20 nm nanodiscs to 400 nm nanosheets. 2D-SupraPol can bind multivalently to the spike protein of SARS-CoV-2, and in-vitro experiments showed that this new 2D supramolecular polymer irreversibly inhibits viral infection while analogs of the polymer that do not self-assemble inhibit the virus reversibly. In-vivo on Syrian hamster studies confirmed the efficacy of intranasal 2D-SupraPol in reducing antiviral infection and accelerating recovery from SARS-CoV-2 infection. We propose 2D supramolecular polymers as a potentially transformative new class of antivirals that can point the way toward effective treatment against a wide range of socially disruptive viruses.

4. Experimental Section

Synthesis of dPG-MUA: dPG-allyl (DF = 100) (50 mg, 0.67 mmol of allyl group), 11-mercaptoundecanoic acid (292.6 mg, 1.34 mmol), 2,2-dimethoxy-2-phenylacetophenone (DMPA) as radical initiator (50 mg, 0.19 mmol) and a catalytic amount of tris(2-carboxyethyl)phosphine hydrochloride (TCEP-HCl) were added to the reaction to avoid oxidation of the thiol intermediate. The solution was degassed by flushing argon through the reaction mixture for 10 min. The reaction mixture was stirred and irradiated with UV light using a high-pressure UV lamp at room temperature for 5 h. The reaction mixture was dialyzed (MWCO 2 kDa) against methanol/chloroform mixture to remove the unreacted chemicals. The solvent mixture was evaporated after the dialysis and product was dissolved in distilled water by adding NaOH 1 M. The excess amount of NaOH was removed by dialysis in water and the final dPG-MUA was achieved after the lyophilization.

Preparation of 2D-SupraPol Solution: 2D-Suprapol was prepared by dissolving dPG-MUA in PBS solution with concentration of 1 mg mL^{-1}.

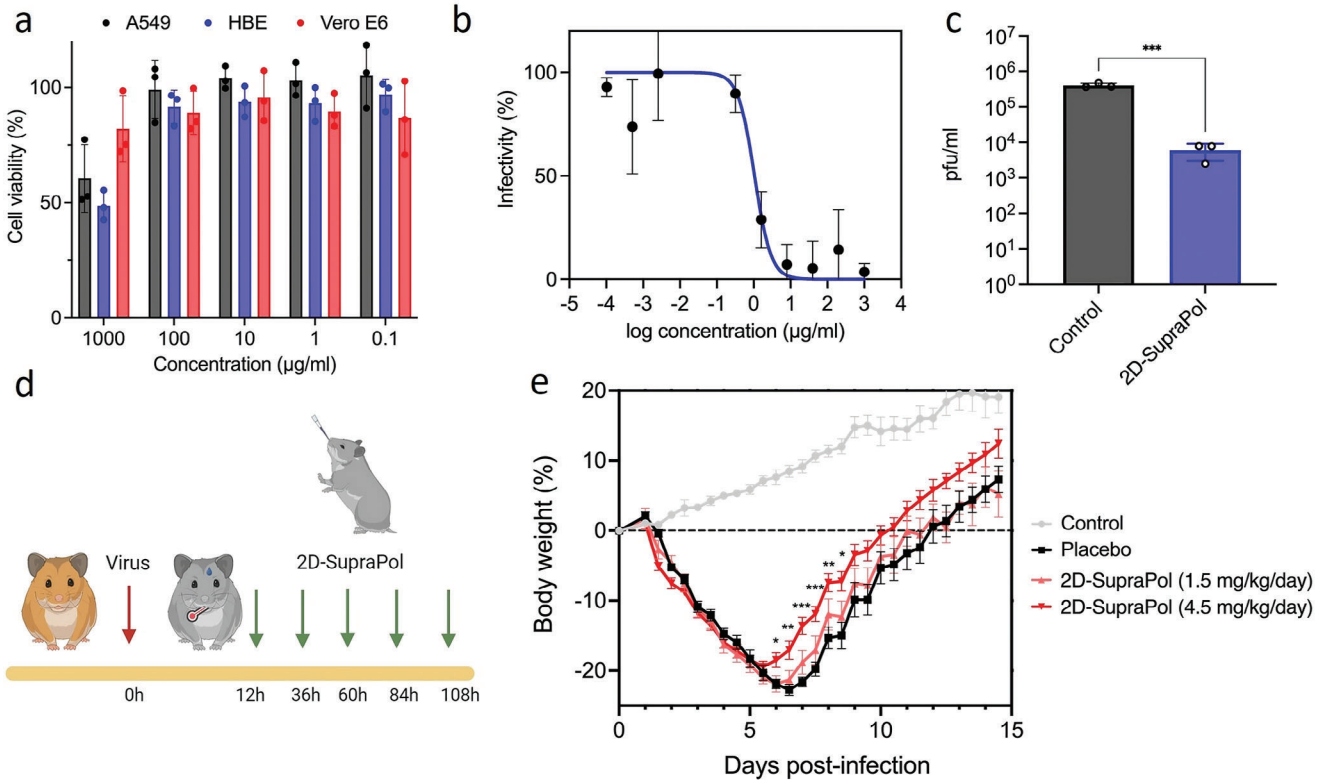

Figure 5. Antiviral activity and cytocompatibility assessment of 2D-SupraPol. a) Cell viability against three different cell lines. Each data point represents the mean of three independent experiments performed in triplicate with standard deviation (±SD). b) Dose response assay against SARS-CoV-2 in Vero E6 cells. Serial dilutions of 2D-SupraPol were incubated for 1 h at 37 °C with SARS-CoV-2 and then added on cells for 2 h at 37 °C. Subsequently, cells were washed and overlaid with medium containing methylcellulose. Plaques were counted 24 h post-infection. Percentages of infections were calculated by comparing the number of plaques in treated and untreated wells. The data is presented as mean ± SD, n = 3. c) Virucidal assays: SARS-CoV-2 was incubated 1 h with media or 2D-SupraPol at 300 µg mL^{-1} and then serially diluted on Vero cells to a negligible concentration of compound. The data is presented as mean ± SD, n = 3. d) Schematic depicting of the animal study design. Created with BioRender.com e) The in vivo results of SARS-CoV-2 inhibition in Hamster. The animals were inoculated by the intranasal route with the live virus and further treatment consisted of intranasal administration of 2D-SupraPol five times at 24 h intervals, starting 12 h after virus inoculation. The data is presented as mean ± SD, n = 10, original data are reported in Figure S16 (Supporting Information). The data were evaluated by one-way ANOVA following Tukey's test using GraphPad Prism software. NS, *, **, and *** represent no significant difference, $P > 0.05$, $p \leq 0.05$, $p < 0.01$, and $p < 0.001$, respectively.

The ionic strength of PBS solution is 152.7 mM containing NaCl:140 mM, KCl:2.7 mM, and PO_4^{3-}:10 mM and pH of solution is 7.4 ± 0.05 at 25 °C. The PBS solution is prepared by dissolving commercially available tablets in milli-Q water. After dissolving the polymer solution is left on the bench at room temperature for 24 h so that the self-assemblies with the lateral size of 200–300 nm are formed.

In Vivo Experiments: All animal experiments described in this study were reviewed and approved by the Institutional Animal Care and Use Committee of the University of Liège (ethical approval no. 21–2370). The "Guide for the Care and Use of Laboratory Animals," prepared by the Institute of Laboratory Animal Resources, National Research Council, and published by the National Academy Press, as well as European and local legislations, was followed carefully. Accordingly, the temperature and relative humidity were 21 °C and 45–60%, respectively. The detailed information about in vivo experiments is presented in the supporting information.

Statistical Analysis: Error bars represent ±SD. Statistical analysis was executed using the GraphPad Prism software (GraphPad Software, Inc., San Diego, CA). Data analysis was performed using SPSS Statistics version 24. The data were analyzed using the one- way ANOVA followed by Tukey's test. NS, *, **, and *** represent no significant difference, $p > 0.05$, $p < 0.05$, $p < 0.01$, and $p < 0.001$, respectively.

Supporting Information

Supporting Information is available from the Wiley Online Library or from the author.

Acknowledgements

Funded by the European Union. Views and opinions expressed are however those of the author(s) only and do not necessarily reflect those of the European Union or the European Research Council Executive Agency. Neither the European Union nor the granting authority can be held responsible for them. This work is supported by ERC grant SupraVir Project Number: 101055416. The research infrastructure SupraFAB (www.suprafab.fu-berlin.de), and the Core Facility BioSupraMol (www.biosupramol.de). The authors acknowledge Benedikt Kirmayer for his assistance with cryo-EM sample preparation. Dr. Jakob Trimpert and Prof. Dr. Benedikt Kaufer are acknowledged for their support with preparation of fixed SARS-CoV-2 virions. The authors would like to thank Elisa Quaas for performing the cell viability assays. The authors thank Denis Puccio for his help with NTA measurement. The authors acknowledge Michael Sztucki and Lauren

Matthews (ESRF Grenoble) for performing USAXS experiments. The authors thank Matthias Ballauf for critical discussion of the constrained fitting procedure. [Correction added on October 11, 2024, after first online publication: Acknowledgements has been updated.]

Open access funding enabled and organized by Projekt DEAL.

Conflict of Interest

This invention is part of the patent application PCT/EP2021/070990 filed on the 27th of July 2021, claiming the priority of EP20 188 654.6, filed on the 30th of July 2020 entitled "Virucidal compositions and use thereof". The inventors of this patent are Matteo Gasbarri, Ehsan Mohammadifar, Francesco Stellacci, and Rainer Haag, and the patent is co-owned by EPFL and FUB.

Author Contributions

R.H. and F.S. initiated the concept, conceived, and designed the experiments. E.M. performed the synthesis and characterizations of supramolecular polymers and contributed to experiment design. M.G. and H.W. contributed to the in vitro SARS-CoV-2 inhibition tests. M.D. and K.L. performed the cryo-TEM and cryo-ET measurements. C.N. purified and provided the SARS-CoV-2 for cryo-TEM measurements. Y.K. performed segmentation of tomogram-based volume reconstructions. T.L.P. performed the MST measurements. S.P. and T.Z. designed the SAXS and SANS experiments, interpreted the data, and proposed the model based on the data. D.D. designed and performed the in vivo experiments.

Data Availability Statement

The data that support the findings of this study are available in the supplementary material of this article.

Keywords

dendritic polymer, SARS-CoV-2, supramolecular structures, virucidal virus inhibition

Received: June 11, 2024
Revised: September 20, 2024
Published online: September 30, 2024

[1] a) G. Morgese, B. F. M. de Waal, S. Varela-Aramburu, A. R. A. Palmans, L. Albertazzi, E. W. Meijer, *Angew. Chem., Int. Ed.* **2020**, *59*, 17229; b) G. Vantomme, E. W. Meijer, *Science.* **2019**, *363*, 1396.

[2] S. P. W. Wijnands, W. Engelen, R. P. M. Lafleur, E. W. Meijer, M. Merkx, *Nat. Commun.* **2018**, *9*, 65.

[3] S. Han, Y.-n. Kim, G. Jo, Y. E. Kim, H. M. Kim, J.-M. Choi, Y. Jung, *Angew. Chem., Int. Ed.* **2020**, *59*, 23244.

[4] P. De Somer, E. De Clercq, A. Billiau, E. Schonne, M. Claesen, *J. Virol.* **1968**, *2*, 878.

[5] A. N. Zelikin, F. Stellacci, *Adv. Healthcare Mater.* **2021**, *10*, 2001433.

[6] a) S. Bhatia, L. C. Camacho, R. Haag, *J. Am. Chem. Soc.* **2016**, *138*, 8654; b) E. Bekerman, S. Einav, *Science.* **2015**, *348*, 282.

[7] a) Z. A. Raza, Q. Shahzad, A. Rehman, M. Taqi, A. Ayub, *3 Biotech.* **2022**, *12*, 273; b) Q. Lin, J. Y. C. Lim, K. Xue, P. Y. M. Yew, C. Owh, P. L. Chee, X. J. Loh, *VIEW.* **2020**, *1*, e16.

[8] a) E. Mohammadifar, M. Gasbarri, V. Cagno, K. Achazi, C. Tapparel, R. Haag, F. Stellacci, *Biomacromolecules.* **2022**, *23*, 983; b) V. Cagno, P. Andreozzi, M. D'Alicarnasso, P. J. Silva, M. Mueller, M. Galloux, R. L.e Goffic, S. T. Jones, M. Vallino, J. Hodek, J. Weber, S. Sen, E.-R. Janeček, A. Bekdemir, B. Sanavio, C. Martinelli, M. Donalisio, M.-A. R. Welti, J.-F. Eleouet, Y. Han, L. Kaiser, L. Vukovic, C. Tapparel, P. Král, S. Krol, D. Lembo, F. Stellacci, *Nat. Mater.* **2018**, *17*, 195; c) S. T. Jones, V. Cagno, M. Janeček, D. Ortiz, N. Gasilova, J. Piret, M. Gasbarri, D. A. Constant, Y. Han, L. Vuković, P. Král, L. Kaiser, S. Huang, S. Constant, K. Kirkegaard, G. Boivin, F. Stellacci, C. Tapparel, *Sci. Adv.* **2020**, *6*, eaax9318.

[9] Y. Xiang, S. Nambulli, Z. Xiao, H. Liu, Z. Sang, W. P. Duprex, D. Schneidman-Duhovny, C. Zhang, Y. Shi, *Science.* **2020**, *370*, 1479.

[10] A. C. Hunt, J. B. Case, Y.-J. Park, L. Cao, K. Wu, A. C. Walls, Z. Liu, J. E. Bowen, H.-W. Yeh, S. Saini, L. Helms, Y. T. Zhao, T.-Y. Hsiang, T. N. Starr, I. Goreshnik, L. Kozodoy, L. Carter, R. Ravichandran, L. B. Green, W. L. Matochko, C. A. Thomson, B. Vögeli, A. Krüger, L. A. VanBlargan, R. E. Chen, B. Ying, A. L. Bailey, N. M. Kafai, S. E. Boyken, A. Ljubetič, et al., *Sci. Transl. Med.* **2022**, *14*, eabn1252.

[11] H. Zhao, K. K. W. To, H. Lam, X. Zhou, J. F.-W. Chan, Z. Peng, A. C. Y. Lee, J. Cai, W.-M. Chan, J. D. Ip, C. C.-S. Chan, M. L. Yeung, A. J. Zhang, A. W. H. Chu, S. Jiang, K.-Y. Yuen, *Nat. Commun.* **2021**, *12*, 1517.

[12] Q. Zhang, A. Honko, J. Zhou, H. Gong, S. N. Downs, J. H. Vasquez, R. H. Fang, W. Gao, A. Griffiths, L. Zhang, *Nano Lett.* **2020**, *20*, 5570.

[13] C. Zhu, J. Y. Lee, J. Z. Woo, L. Xu, X. Nguyenla, L. H. Yamashiro, F. Ji, S. B. Biering, E. Van Dis, F. Gonzalez, D. Fox, E. Wehri, A. Rustagi, B. A. Pinsky, J. Schaletzky, C. A. Blish, C. Chiu, E. Harris, R. I. Sadreyev, S. Stanley, S. Kauppinen, S. Rouskin, A. M. Näär, *Nat. Commun.* **2022**, *13*, 4503.

[14] B. Ju, Q. Zhang, J. Ge, R. Wang, J. Sun, X. Ge, J. Yu, S. Shan, B. Zhou, S. Song, X. Tang, J. Yu, J. Lan, J. Yuan, H. Wang, J. Zhao, S. Zhang, Y. Wang, X. Shi, L. Liu, J. Zhao, X. Wang, Z. Zhang, L. Zhang, *Nature.* **2020**, *584*, 115.

[15] a) Z. Tang, N. Kong, X. Zhang, Y. Liu, P. Hu, S. Mou, P. Liljeström, J. Shi, W. Tan, J. S. Kim, Y. Cao, R. Langer, K. W. Leong, O. C. Farokhzad, W. Tao, *Nat. Rev. Mater.* **2020**, *5*, 847; b) M. Sun, S. Liu, T. Song, F. Chen, J. Zhang, J.-a. Huang, S. Wan, Y. Lu, H. Chen, W. Tan, Y. Song, C. Yang, *J. Am. Chem. Soc.* **2021**, *143*, 21541; c) X. Huang, E. Kon, X. Han, X. Zhang, N. Kong, M. J. Mitchell, D. Peer, W. Tao, *Nat. Nanotechnol.* **2022**, *17*, 1027.

[16] M. Gasbarri, P. V'kovski, G. Torriani, V. Thiel, F. Stellacci, C. Tapparel, V. Cagno, *Microorganisms* **2020**, *8*, 1984.

[17] a) L. Gu, Z. Duan, X. Chen, X. Li, Q. Luo, A. Bhamra, D. Pan, H. Zhu, X. Tian, R. Chen, Z. Gu, H. Zhang, Z. Qian, Q. Gong, K. Luo, *Adv. Mater.* **2022**, *34*, 2200048; b) Y. Zhang, Z. Fang, D. Pan, Y. Li, J. Zhou, H. Chen, Z. Li, M. Zhu, C. Li, L. Qin, X. Ren, Q. Gong, K. Luo, *Adv. Mater.* **2024**, *36*, 2401304.

[18] a) P. Dey, T. Bergmann, J. L. Cuellar-Camacho, S. Ehrmann, M. S. Chowdhury, M. Zhang, I. Dahmani, R. Haag, W. Azab, *ACS Nano.* **2018**, *12*, 6429; b) S. Bhatia, M. Hilsch, J. L. Cuellar-Camacho, K. Ludwig, C. Nie, B. Parshad, M. Wallert, S. Block, D. Lauster, C. Böttcher, A. Herrmann, R. Haag, *Angew. Chem., Int. Ed.* **2020**, *59*, 12417; c) E. Mohammadifar, V. Ahmadi, M. F. Gholami, A. Oehrl, O. Kolyvushko, C. Nie, I. S. Donskyi, S. Herziger, J. Radnik, K. Ludwig, C. Böttcher, J. P. Rabe, K. Osterrieder, W. Azab, R. Haag, M. Adeli, *Adv. Funct. Mater.* **2021**, *31*, 2009003; d) R. Bej, C. Nie, K. Ludwig, V. Ahmadi, J. Trimpert, J. M. Adler, T. L. Povolotsky, K. Achazi, M. Kagelmacher, R. M. Vidal, J. Dernedde, B. B. Kaufer, R. Haag, *Angew. Chem., Int. Ed.* **2023**, *62*, 202304010.

[19] G. Zhang, Y. Cong, F.-L. Liu, J. Sun, J. Zhang, G. Cao, L. Zhou, W. Yang, Q. Song, F. Wang, K. Liu, J. Qu, J. Wang, M. He, S. Feng, D. Baimanov, W. Xu, R.-H. Luo, X.-Y. Long, S. Liao, Y. Fan, Y.-F. Li, B. Li, X. Shao, G. Wang, L. Fang, H. Wang, X.-F. Yu, Y.-Z. Chang, Y. Zhao, et al., *Nat. Nanotechnol.* **2022**, *17*, 993.

[20] B. Rad, T. K. Haxton, A. Shon, S.-H. Shin, S. Whitelam, C. M. Ajo-Franklin, *ACS Nano*. **2015**, *9*, 180.
[21] T. Kim, J. Y. Park, J. Hwang, G. Seo, Y. Kim, *Adv. Mater.* **2020**, *32*, 2002405.
[22] Y. Ni, J. Sun, Y. Wei, X. Fu, C. Zhu, Z. Li, *Biomacromolecules*. **2017**, *18*, 3367.
[23] M. A. Hartmann, R. Weinkamer, T. Zemb, F. D. Fischer, P. Fratzl, *Phys. Rev. Lett.* **2006**, *97*, 018106.
[24] O. Glatter, in *Scattering Methods and their Application in Colloid and Interface Science*, (Ed.: O. Glatter), Elsevier, New York **2018**, 1.
[25] E. Y. Sheu, P. Lo Nostro, G. Capuzzi, P. Baglioni, *Langmuir.* **1999**, *15*, 6671.
[26] B. Cabane, R. Duplessix, T. Zemb, *J. Phys. France.* **1985**, *46*, 2161.
[27] J. Chen, C. L. Brooks, H. A. Scheraga, *J. Phys. Chem. B.* **2008**, *112*, 242.
[28] a) L. Liu, P. Chopra, X. Li, K. M. Bouwman, S. M. Tompkins, M. A. Wolfert, R. P. de Vries, G.-J. Boons, *ACS Cent. Sci.* **2021**, *7*, 1009; b) R. Groß, L. M. Dias Loiola, L. Issmail, N. Uhlig, V. Eberlein, C. Conzelmann, L.-R. Olari, L. Rauch, J. Lawrenz, T. Weil, J. A. Müller, M. B. Cardoso, A. Gilg, O. Larsson, U. Höglund, S. A. Pålsson, A. S. Tvilum, K. B. Løvschall, M. M. Kristensen, A.-L. Spetz, F. Hontonnou, M. Galloux, T. Grunwald, A. N. Zelikin, J. Münch, *Adv. Sci.* **2022**, *9*, 2201378; c) Q. Zhang, C. Z. Chen, M. Swaroop, M. Xu, L. Wang, J. Lee, A. Q. Wang, M. Pradhan, N. Hagen, L. Chen, M. Shen, Z. Luo, X. Xu, Y. Xu, W. Huang, W. Zheng, Y. Ye, *Cell Discov.* **2020**, *6*, 80.
[29] C. Nie, P. Pouyan, D. Lauster, J. Trimpert, Y. Kerkhoff, G. P. Szekeres, M. Wallert, S. Block, A. K. Sahoo, J. Dernedde, K. Pagel, B. B. Kaufer, R. R. Netz, M. Ballauff, R. Haag, *Angew. Chem., Int. Ed.* **2021**, *60*, 15870.
[30] S. T. Jones, V. Cagno, M. Janeček, D. Ortiz, N. Gasilova, J. Piret, M. Gasbarri, D. A. Constant, Y. Han, L. Vuković, P. Král, L. Kaiser, S. Huang, S. Constant, K. Kirkegaard, G. Boivin, F. Stellacci, C. Tapparel, *Sci. Adv. 6*, eaax9318.
[31] M. Gasbarri, Ph.D. Thesis, , EPFL (Lausanne), **2021**.
[32] J. Lan, J. Ge, J. Yu, S. Shan, H. Zhou, S. Fan, Q. Zhang, X. Shi, Q. Wang, L. Zhang, X. Wang, *Nature.* **2020**, *581*, 215.
[33] D. Wrapp, N. Wang, K. S. Corbett, J. A. Goldsmith, C.-L. Hsieh, O. Abiona, B. S. Graham, J. S. McLellan, *Science.* **2020**, *367*, 1260.